Mechanics Research Communications 125 (2022) 103978

Contents lists available at ScienceDirect

Mechanics Research Communications

journal homepage: www.elsevier.com/locate/mechrescom

An energy-based strategy to find admissible thrust networks compatible with foundation settlements in masonry structures

R. Maia Avelino [a,*], A. Iannuzzo [b], T. Van Mele [a], P. Block [a]

[a] ETH Zurich, Department of Architecture, Block Research Group, Stefano-Franscini-Platz 1, HIB E 45, Zurich, 8093, Switzerland
[b] Swinburne University of Technology, Department of Civil and Construction Engineering and Department of Architectural and Industrial Design, Melbourne, VIC 3122, Australia

ARTICLE INFO

Keywords:
Limit analysis
Thrust network analysis
Complementary energy
Foundation settlements
Cracks

ABSTRACT

This paper presents an energy-based methodology to compute internal stress states compatible with foundation settlements in masonry structures. The method is based on the application of Thrust Network Analysis (TNA). TNA is a lower-bound method that searches for admissible force networks in masonry structures by solving a constrained nonlinear optimisation problem (NLP) in which constraints enforce the limit analysis' admissibility criteria. In this paper, the objective function minimises the complementary energy, which directly considers prescribed foundation displacements. This minimum energy criterion allows selecting among the infinite admissible stress states, the ones compatible with the settlements, suggesting potential crack regions at the onset of the motion. Application to general two- and three-dimensional masonry structures under vertical and horizontal loads are presented. The method has the potential to link internal stress states to boundary displacements and, thus, give mechanical meaning to typical crack patterns observed in masonry structures.

1. Introduction

The mechanics of masonry structures are dictated by their discrete nature and negligible tensile capacity [1]. Due to this unilateral behaviour, the stability in masonry relies primarily on structural geometry rather than material strength [2]. Unlike elastic systems, foundation settlements or excessive loads lead to the development of cracks and the creation of rigid macro-blocks [3]. These particularities preclude the application of general analysis tools to masonry buildings, enforcing the need for suitable analysis methods, which are currently scarce [4,5].

Adopting Heyman's assumptions [6], limit analysis can be applied to masonry structures [7–11]. In continuum mechanics, these hypotheses have been formalised in [12,13]. Prior to this formal description, internal stresses were searched by finding compressive paths within the envelope of two-dimensional structures in combination with graphic statics [14–17]. Currently, this technique is known as Thrust Line Analysis (TLA) and has a series of 2D or pseudo-3D applications [18–20].

For general three-dimensional structures, following the work of [21], Thrust Network Analysis (TNA) was proposed in [22] as an extension of TLA which considers the internal stresses as an axial force network. It decouples horizontal and vertical network equilibria, computed by solving two successive linear optimisation problems. In [23], horizontal forces are introduced. In [24], the network's horizontal projection, or form diagram, is fixed, reducing the indeterminacy of the equilibrium and allowing for efficiently coupling of the horizontal and vertical equilibria in a direct optimisation process. Further work [25–28] introduced different objective functions, such as minimising and maximising the horizontal thrust and maximising the geometric safety factor (GSF) and imposed constraints to the network's vertex elevations to lay within the structure. These later developments enabled the application of TNA to practical masonry assessment problems, keeping as main advantages the simple and intuitive input necessary to the analysis: the structural envelope and the geometry of the form diagram.

Nevertheless, one of the major challenges when assessing existing structures is associating the observed cracks, or pathologies, with foundation settlements [29,30]. This can be done by introducing an energy-based criterion that minimises the complementary energy of the structure for a given foundation displacement [13]. This approach has been applied to a normal, rigid, no-tension (NRNT) material in [31], with applications to 2D structures [32,33] or to panels [34,35] assuming an elastic response in compression. It is shown that for a NRNT material, minimising the complementary energy is equal to minimising the opposite work of the reaction forces [33].

In this paper, the TNA formulation is revisited and coupled, for the first time, with the complementary energy minimisation. The present formulation can deal with vertical and horizontal loading conditions,

* Corresponding author.
E-mail addresses: maia@arch.ethz.ch (R. Maia Avelino), aiannuzzo@swin.edu.au (A. Iannuzzo).

https://doi.org/10.1016/j.mechrescom.2022.103978
Received 13 July 2022; Received in revised form 25 August 2022; Accepted 4 September 2022
Available online 6 September 2022

and, unlike previous approaches, such as [32,34], it applies to any spatial geometry. By searching among infinite admissible stress states, the ones compatible with specific settlements, the locations where cracks are most likely to form following these movements are revealed. The outcome helps to understand the mechanical behaviour of vaulted masonry structures through a comprehensive analysis method that practitioners can readily use.

The paper is organised as follows: Section 2 revisits the TNA formulation. Section 3 couples the search of admissible thrust networks with the minimisation of the complementary energy. Section 4 shows applications to two- and three-dimensional structures, followed by a discussion in Section 5 and the conclusions in Section 6.

2. Thrust network analysis

In this section, the methodology to compute spatial thrust networks is presented 2.1, the particular case for fixed network projection is introduced 2.2 and the limit analysis TNA constraints are formalised 2.3.

2.1. Equilibrium networks

The solutions considered consist of a connected network composed of m edges and n vertices, partitioned in n_i internal and n_b support vertices. Nodal positions are collected in vectors $\mathbf{x}, \mathbf{y}, \mathbf{z}$ $[n \times 1]$ and applied loads at each direction in $\mathbf{p}_\mathrm{x}, \mathbf{p}_\mathrm{y}, \mathbf{p}_\mathrm{z}$ $[n \times 1]$. The edge force densities $\mathbf{q}$ $[m \times 1]$ are taken as the static variables of the problem and are defined at an edge i as the ratio among its axial force f_i and the edge length l_i, as in [36].

With this formulation, the nodal equilibrium of a network can be written by introducing the connectivity matrix $\mathbf{C}$ $[m \times n]$ representing the connectivity and orientation of the edges in the network and the coordinate difference matrices $\mathbf{U} = \mathrm{diag}(\mathbf{Cx})$, $\mathbf{V} = \mathrm{diag}(\mathbf{Cy})$, $\mathbf{W} = \mathrm{diag}(\mathbf{Cz})$ $[m \times m]$. Let $\mathbf{C}_\mathrm{i}$ $[m \times n_\mathrm{i}]$ represent the slice of $\mathbf{C}$ in the free nodes, the $3n_\mathrm{i}$ internal equilibrium equations are

$$\mathbf{C}_\mathrm{i}^\mathrm{T}\mathbf{U}\mathbf{q} = \mathbf{p}_\mathrm{x,i}, \tag{1a}$$

$$\mathbf{C}_\mathrm{i}^\mathrm{T}\mathbf{V}\mathbf{q} = \mathbf{p}_\mathrm{y,i}, \tag{1b}$$

$$\mathbf{C}_\mathrm{i}^\mathrm{T}\mathbf{W}\mathbf{q} = \mathbf{p}_\mathrm{z,i}. \tag{1c}$$

2.2. Networks with fixed horizontal projection

In this work, networks with fixed horizontal projections are considered. This projection corresponds to a planar, connected graph named form diagram. As a consequence, the horizontal equilibrium equations (Eqs. (1a) and (1b)) are rearranged, introducing the horizontal equilibrium matrix $\mathbf{E} = (\mathbf{C}_\mathrm{i}^\mathrm{T}\mathbf{U}; \mathbf{C}_\mathrm{i}^\mathrm{T}\mathbf{V})$ $[2n_\mathrm{i} \times m]$ and the applied horizontal internal forces $\mathbf{p}_\mathrm{h,i} = (\mathbf{p}_\mathrm{x,i}; \mathbf{p}_\mathrm{y,i})$ $[2n_\mathrm{i} \times 1]$. By exploiting the structure of the null-space of $\mathbf{E}$, the force densities are re-parametrised and written as a function of k independent force densities $\mathbf{q}_\mathrm{id}$ as

$$\mathbf{q} = \mathbf{B}\mathbf{q}_\mathrm{id} + \mathbf{d}, \text{ with: } \mathbf{B} = \begin{bmatrix} -\mathbf{E}_\mathrm{d}^\dagger\mathbf{E}_\mathrm{id} \\ \mathbf{I}_\mathrm{k} \end{bmatrix}, \mathbf{d} = \begin{bmatrix} \mathbf{E}_\mathrm{d}^\dagger\mathbf{p}_\mathrm{h,i} \\ \mathbf{0} \end{bmatrix}, \tag{2}$$

where $\mathbf{I}_\mathrm{k}$ is the identity matrix of size k, $\mathbf{E}_\mathrm{d}$ and $\mathbf{E}_\mathrm{id}$ are slices of $\mathbf{E}$ related to the dependent and independent edges, respectively, and $\mathbf{E}_\mathrm{d}^\dagger$ is the generalised inverse or Moore–Penrose pseudo-inverse of $\mathbf{E}_\mathrm{d}$.

The transformation adopted in Eq. (2) allows for a variable reduction and for exploring the network equilibrium while keeping the form diagram projection unchanged. A selected group of k independent edges (resp. $m - k$ dependent edges) relates with the independent force densities $\mathbf{q}_\mathrm{id}$ (resp. dependent force densities $\mathbf{q}_\mathrm{d}$). The number of independent edges in a planar form diagram corresponds to its degrees of freedom (DOFs) [37,38].

Through this formulation, the infinite space of spatial networks for a given form diagram geometry can be explored. The elevation of the free nodes in the network $\mathbf{z}_\mathrm{i}$ are then described as a function of $\mathbf{q}_\mathrm{id}$ and the support elevations $\mathbf{z}_\mathrm{b}$,

$$\mathbf{z}_\mathrm{i}\left(\mathbf{q}_\mathrm{id}, \mathbf{z}_\mathrm{b}\right) = \mathbf{D}_\mathrm{i}^{-1}\left(\mathbf{p}_\mathrm{z,i} - \mathbf{D}_\mathrm{b}\mathbf{z}_\mathrm{b}\right), \tag{3}$$

with $\mathbf{D}_\mathrm{i} = \mathbf{C}_\mathrm{i}^\mathrm{T}\mathbf{Q}\mathbf{C}_\mathrm{i}$ $[n_\mathrm{i} \times n_\mathrm{i}]$, $\mathbf{D}_\mathrm{b} = \mathbf{C}_\mathrm{i}^\mathrm{T}\mathbf{Q}\mathbf{C}_\mathrm{b}$ $[n_\mathrm{i} \times n_\mathrm{b}]$ and $\mathbf{Q} = \mathrm{diag}(\mathbf{q})$ $[m \times m]$.

2.3. Admissible networks

As described in [6], limit analysis can be applied to masonry structures, given that infinite compressive strength and null tensile strength are assumed, and no sliding failure can occur. In continuum mechanics, these assumptions are generalised in applying the normal, rigid, no-tension material (NRNT) described in [31]. For the present formulation, these assumptions translate into no-tensile axial forces at the network edges and constrain the network to remain within the structural section. The former enforces negative axial force densities q_i in the edges (Eq. (4a)) and the latter is implemented by constraining the nodal elevations z_i to lay between the elevations of intrados z_i^LB and extrados z_i^UB (Eq. (4b)).

$$q_i \le 0 \qquad \text{for} \qquad i = [1, \dots, m], \tag{4a}$$

$$z_i^\mathrm{LB} \le z_i \le z_i^\mathrm{UB} \qquad \text{for} \qquad i = [1, \dots, n]. \tag{4b}$$

Remark 1. To check the no-sliding assumption, from Heyman [6], a stereotomy and friction coefficient must be assumed to discretise the continuous domain. In the present methodology, the masonry is assumed as a continuous envelope. For adaptations of the methodology considering interfaces, the readers are referred to [39,40].

Remark 2. Nevertheless, as shown in [40], if a specific stereotomy is coupled with the TNA approach, the formulation is equivalent to assuming a vertical stereotomy to the blocks. This is clearly a conservative assumption which is far from the typical well-constructed historical masonry vaults as claimed in [2,41].

3. An energy-based criterion for NRNT material

In this section, the complementary energy formulation is revisited in the context of reticulated systems 3.1. It is then specialised in the NRNT model 3.2 and coupled with the search for admissible thrust networks 3.3.

3.1. Complementary energy for a discrete network

We recall the Complementary Energy W_c expression from [13], for a continuum $\Omega \in \mathbb{R}^3$. On the constrained boundary $\delta\Omega_\mathrm{D}$, prescribed displacements $\bar{\mathbf{u}}$ are applied, and the internal stresses are represented by the tensor $\mathbf{T}$. Let $\mathbf{A}$ be the fourth order tensor modelling a linear hyperelastic behaviour in compression, the expression is

$$W_\mathrm{c} = -\int_{\delta\Omega_\mathrm{D}} \mathbf{T}\cdot\bar{\mathbf{u}}\, ds + \frac{1}{2}\int_\Omega \mathbf{A}\mathbf{T} : \mathbf{T}\, dV. \tag{5}$$

The first term in Eq. (5) is linear and accounts for the imposed displacements on the supports. The second, quadratic term reflects the internal energy of the structure. Assuming a discretisation into a reticulated system, the internal energy simplifies to its axial component, which for an elastic material is written by introducing the structure's Young modulus E and the cross-sectional areas A_i. Assuming that the ratio f_i/A_i is constant within the structure, i.e., the cross-section areas A_i are proportional to the axial force f_i, the expression can be further simplified and written in terms of the force densities q_i as

$$\frac{1}{2}\int_\Omega \mathbf{A}\mathbf{T} : \mathbf{T}\, dV = \sum_i^m \frac{f_i^2\, l_i}{2\, E\, A_i} = \frac{1}{2\epsilon}\sum_i^m |q_i|\, l_i^2, \tag{6}$$

in which, the constant ϵ takes into account the stiffness and the axial strength in the bars of the structure. Eq. (6) yields in the well-known load-path [42–44], which is linear for a system with given bar lengths but nonlinear in the present case where the lengths are a function of the nodal elevations.

Remark 3. In fact, as demonstrated in [42], the term in Eq. (6) is convex assuming that (i) the network horizontal projection is fixed, (ii) the supports are co-planar, and (iii) unilateral forces are considered.

Therefore, the expression of the complementary energy in a reticular system with stiffness parameter ϵ for a given set of support displacements $\bar{\mathbf{u}}$ $[n \times 3]$ is

$$\tilde{W}_{\mathrm{c}}(\bar{\mathbf{u}}, \epsilon) = -\sum_{i}^{n_{\mathrm{b}}} \mathbf{R}_i \cdot \bar{\mathbf{u}}_i + \frac{1}{2\epsilon} \sum_{i}^{m} |q_i| * l_i^2, \tag{7}$$

in which, the reaction forces in the support i $\mathbf{R}_i = [R_{\mathrm{x},i};\ R_{\mathrm{y},i};\ R_{\mathrm{z},i}]$ can be retrieved from the components $\mathbf{R}_{\mathrm{x}}$, $\mathbf{R}_{\mathrm{y}}$, $\mathbf{R}_{\mathrm{z}}$ $[n_{\mathrm{b}} \times 1]$ calculated as

$$\mathbf{R}_{\mathrm{x}} = \mathbf{C}_{\mathrm{b}}^{\mathrm{T}}\mathbf{U}\mathbf{q} - \mathbf{p}_{\mathrm{x,b}}, \tag{8a}$$

$$\mathbf{R}_{\mathrm{y}} = \mathbf{C}_{\mathrm{b}}^{\mathrm{T}}\mathbf{V}\mathbf{q} - \mathbf{p}_{\mathrm{y,b}}, \tag{8b}$$

$$\mathbf{R}_{\mathrm{z}} = \mathbf{C}_{\mathrm{b}}^{\mathrm{T}}\mathbf{W}\mathbf{q} - \mathbf{p}_{\mathrm{z,b}}. \tag{8c}$$

The horizontal components of the reaction forces (Eqs. (8a) and (8b)) are a linear function of $\mathbf{q}_{\mathrm{id}}$, while $\mathbf{R}_{\mathrm{z}}$ is a function of the unknown elevations of the network $\mathbf{z}$ and, therefore, a function of both $\mathbf{q}_{\mathrm{id}}$ and $\mathbf{z}_{\mathrm{b}}$.

3.2. Network complementary energy for NRNT model

For the normal, rigid, no-tensile NRNT model, the internal elastic energy in Eq. (7) vanishes. This is equivalent to assuming that the stiffness parameter in the network bars is infinite ($\epsilon \to \infty$), such that the complementary energy expression simplifies to:

$$\tilde{W}_{\mathrm{c}}^{\mathrm{NRNT}}(\bar{\mathbf{u}}) = \tilde{W}_{\mathrm{c}}(\bar{\mathbf{u}}, \epsilon \to \infty) = -\sum_{i}^{n_{\mathrm{b}}} \mathbf{R}_i \cdot \bar{\mathbf{u}}_i \tag{9}$$

3.3. Minimising the complementary energy in the set of admissible thrust networks

The search for the admissible stress solutions minimising the complementary energy in masonry structures for given foundation displacements $\bar{\mathbf{u}}$ is then executed by formulating and solving the following nonlinear optimisation problem (NLP):

$$\underset{\mathbf{q}_{\mathrm{id}}, \mathbf{z}_{\mathrm{b}}}{\text{minimise}} \quad \tilde{W}_{\mathrm{c}}^{\mathrm{NRNT}}(\bar{\mathbf{u}}), \tag{10a}$$

$$\text{subject to} \quad q_i \le 0, \quad \text{for } i = [1, \dots, m], \tag{10b}$$

$$z_i^{\mathrm{LB}} \le z_i \le z_i^{\mathrm{UB}}, \quad \text{for } i = [1, \dots, n], \tag{10c}$$

in which, the variables are the independent force densities $\mathbf{q}_{\mathrm{id}}$, and the support elevations $\mathbf{z}_{\mathrm{b}}$ from Section 2. The problem's nonlinearity comes from imposing the nodal elevations to remain between the intrados and extrados of the masonry (Eq. (10c)). The objective function is linear in terms of the reaction forces computed with Eq. (8).

The optimisation in Eq. (10) can be solved using interior point methods. In this paper, the implementation is based on the open-source solver IPOPT [45], which is wrapped in the *compas_tno* [46] package developed by the authors. As a starting point to the NLP, a convex problem is formulated minimising Eq. (6) to find the minimal load path compressive network (see Remark 3), as in [42].

The description of the Jacobian matrix of the constraints is available in [25]. The gradient of the objective function over the problem variables $\partial\tilde{W}_{\mathrm{c}}^{\mathrm{NRNT}}/\partial\mathbf{q}_{\mathrm{id}}$ $[k \times 1]$ and $\partial\tilde{W}_{\mathrm{c}}^{\mathrm{NRNT}}/\partial\mathbf{z}_{\mathrm{b}}$ $[n_{\mathrm{b}} \times 1]$ is written in terms of the partial derivatives of the reaction forces $\partial\mathbf{R}_{\mathrm{z}}/\partial\mathbf{q}_{\mathrm{id}}$ $[n_{\mathrm{b}} \times k]$ and $\partial\mathbf{R}_{\mathrm{z}}/\partial\mathbf{z}_{\mathrm{b}}$ $[n_{\mathrm{b}} \times n_{\mathrm{b}}]$ (and resp. x, y) as

$$\frac{\partial\tilde{W}_{\mathrm{c}}^{\mathrm{NRNT}}}{\partial\mathbf{q}_{\mathrm{id}}} = -\left[\frac{\partial\mathbf{R}_{\mathrm{x}}}{\partial\mathbf{q}_{\mathrm{id}}}^{\mathrm{T}}, \frac{\partial\mathbf{R}_{\mathrm{y}}}{\partial\mathbf{q}_{\mathrm{id}}}^{\mathrm{T}}, \frac{\partial\mathbf{R}_{\mathrm{z}}}{\partial\mathbf{q}_{\mathrm{id}}}^{\mathrm{T}}\right]\begin{bmatrix}\bar{\mathbf{u}}_{\mathrm{x}}\\ \bar{\mathbf{u}}_{\mathrm{y}}\\ \bar{\mathbf{u}}_{\mathrm{z}}\end{bmatrix}, \tag{11a}$$

$$\frac{\partial\tilde{W}_{\mathrm{c}}^{\mathrm{NRNT}}}{\partial\mathbf{z}_{\mathrm{b}}} = -\frac{\partial\mathbf{R}_{\mathrm{z}}}{\partial\mathbf{z}_{\mathrm{b}}}^{\mathrm{T}}\bar{\mathbf{u}}_{\mathrm{z}} \tag{11b}$$

in which, $\bar{\mathbf{u}}_{\mathrm{x}}, \bar{\mathbf{u}}_{\mathrm{y}}, \bar{\mathbf{u}}_{\mathrm{z}}$ $[n \times 1]$ represent the x, y, z components of the support displacement and the partial derivatives of the reaction forces are expressed below (see also [25]):

$$\frac{\partial\mathbf{R}_{\mathrm{x}}}{\partial\mathbf{q}_{\mathrm{id}}} = \mathbf{C}_{\mathrm{b}}^{\mathrm{T}}\mathbf{U}\mathbf{B}, \tag{12a}$$

$$\frac{\partial\mathbf{R}_{\mathrm{y}}}{\partial\mathbf{q}_{\mathrm{id}}} = \mathbf{C}_{\mathrm{b}}^{\mathrm{T}}\mathbf{V}\mathbf{B}, \tag{12b}$$

$$\frac{\partial\mathbf{R}_{\mathrm{z}}}{\partial\mathbf{q}_{\mathrm{id}}} = \mathbf{C}_{\mathrm{b}}^{\mathrm{T}}\mathbf{W}\mathbf{B} + \mathbf{C}_{\mathrm{b}}^{\mathrm{T}}\mathbf{Q}\mathbf{C}\begin{bmatrix}-\mathbf{D}_{\mathrm{i}}^{-1}\mathbf{C}_{\mathrm{i}}^{\mathrm{T}}\mathbf{W}\mathbf{B}\\ \mathbf{0}\end{bmatrix}, \tag{12c}$$

$$\frac{\partial\mathbf{R}_{\mathrm{z}}}{\partial\mathbf{z}_{\mathrm{b}}} = \mathbf{C}_{\mathrm{b}}^{\mathrm{T}}\mathbf{Q}\mathbf{C}\begin{bmatrix}-\mathbf{D}_{\mathrm{i}}^{-1}\mathbf{D}_{\mathrm{b}}\\ \mathbf{I}_{n_{\mathrm{b}}}\end{bmatrix}. \tag{12d}$$

4. Results

Relevant two- and three-dimensional examples are presented in this section to illustrate the range of applications of the proposed methodology.

4.1. Validation on the semicircular arch

The first application refers to a semicircular arch with thickness over (central) radius $t/R_{\mathrm{c}} = 0.20$ (Fig. 1a). A linear form diagram with 50 nodes is used in the analysis with supports at both extremities. The self-weight (W) is lumped into the nodes of the diagram according to its tributary areas after projection in the arch's central geometry. The arch is subjected to three sets of settlements $\bar{\mathbf{u}}_i$ applied to the right support: outwards $\bar{\mathbf{u}}_1 = [1, 0]$, inwards $\bar{\mathbf{u}}_2 = [-1, 0]$, and downwards $\bar{\mathbf{u}}_3 = [0, -1]$. For each case, the optimisation problem in Eq. (10) is solved, and the results are presented in Fig. 1b–d. In the plots, the points in which the thrust line touch intrados and extrados are highlighted with blue and green dots. When the thrust line touches the intrados (resp. extrados), a crack forms on the extrados (resp. intrados). Additional constraints preventing the extension of the emerging reactions from crossing the extrados are activated as in [25].

For the outward and inward displacement (Figs. 1b–c), the arch assumes the well-known minimum and maximum thrust states [29,41, 47]. The normalised horizontal reaction in one support is $T_{\min}/W = 15.8\%$ and $T_{\max}/W = 25.5\%$. The downward settlement (Fig. 1d) produces a tilted thrust line with uneven vertical reaction forces. The vertical component of the settled support is reduced to $V_{\mathrm{R}}/W = 47.8\%$ and the horizontal thrust is $T_{\mathrm{down}}/W = 18.9\%$. This analysis confirms results obtained in [48,49], validating the method and evidencing its intuitive physical result.

4.2. Hemispheric dome

In this section, a hemispheric dome is analysed. The geometry of the dome is obtained through a revolution of the circular section in Fig. 1a, with $t/R_{\mathrm{c}} = 0.10$. Two different diagrams are considered to perform the analysis. A radial continuously supported form diagram composed of 20 meridians and 16 hoops (Fig. 2a), and a modified diagram, with the same 20 supports but with inclined meridians, not converging to the centre (Fig. 2b). The independent edges and supports for the diagrams are highlighted in Figs. 2a–b. The dome is subjected to

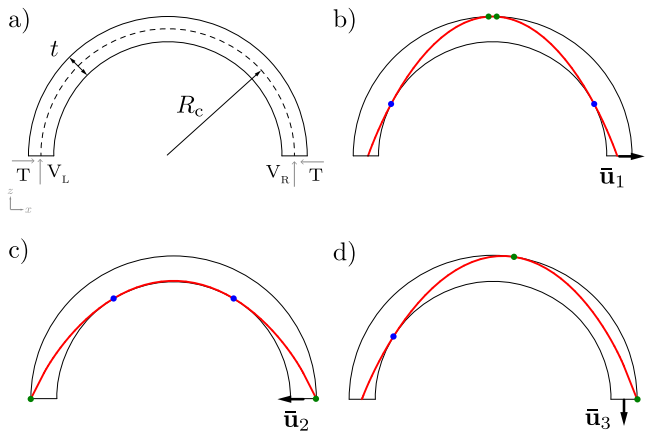

Fig. 1. (a) Geometry of the semicircular arch and notation of reaction forces. Minimum complementary energy solution for a displacement (a) outward $\bar{\mathbf{u}}_1$, (b) inward $\bar{\mathbf{u}}_2$ and (c) downward $\bar{\mathbf{u}}_3$ imposed to the right support. (For interpretation of the references to colour in this figure legend, the reader is referred to the web version of this article.)

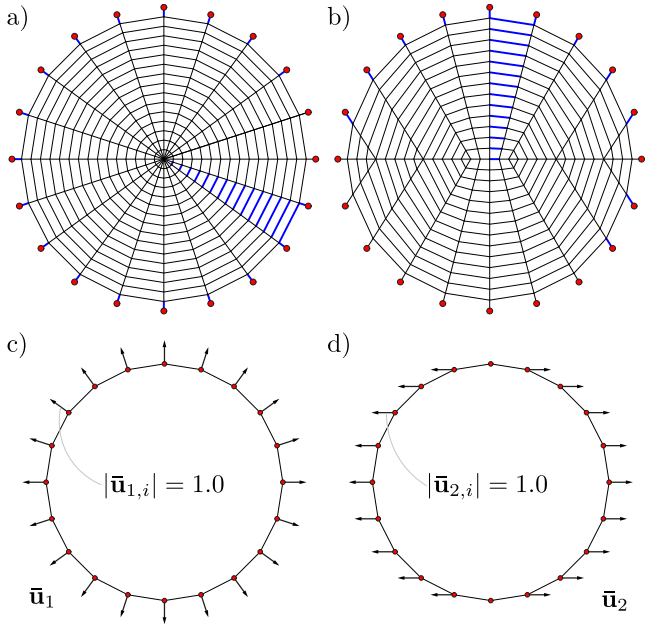

Fig. 2. Form diagrams used in the hemispheric dome analysis: (a) radial diagram (b) modified diagram. Supports are shown in red and independent edges in blue. (a) Spreading $\bar{\mathbf{u}}_1$ and (b) splitting $\bar{\mathbf{u}}_2$ displacement fields applied to the supports. (For interpretation of the references to colour in this figure legend, the reader is referred to the web version of this article.)

two sets of unitary foundation displacements. A spreading displacement $\bar{\mathbf{u}}_1$ (Fig. 2c), and a splitting displacement $\bar{\mathbf{u}}_2$ dividing the dome into two halves (Fig. 2d).

The results obtained are reported in Fig. 3, in which the thrust network (G) is shown next to the reciprocal form (Γ) and force (Γ^*) diagrams. The force diagram represents the internal equilibrium [22]. Each edge in Γ^* maps to an orthogonal edge in Γ such that the magnitude of the horizontal force carried by the latter corresponds to the length of the former. The scale of Γ^* is reported as a percentage of the dome's self-weight (W). The thickness of the edges in G and Γ are scaled to the force carried.

Fig. 3a shows the minimum of the complementary energy once the spreading displacement $\bar{\mathbf{u}}_1$ has been applied to the radial diagram. The normalised objective function reported is $\tilde{W}_c/W = 19.9\%$. In the solution obtained, a bi-axial compression cap is seen in the upper part of the dome, and a uniaxial stress field appears near the supports. The uniaxial state indicates the well-known meridian cracks for the spreading collapse mechanism of the dome [41]. Two cylindrical crack lines can be identified by neighbouring vertices touching the intrados (blue) and the extrados (green). In Γ^*, the lengths of the perimetral edges measure the magnitude of the radial horizontal thrust emerging (e.g., T_i) and, therefore, the perimeter of Γ^* corresponds to $\tilde{W}_c$ for the spreading displacement. The optimal complementary energy value also matches the result of minimum normalised horizontal thrusts from [25,40], showing that these solutions are equivalent.

The solution in Fig. 3b shows the thrust network obtained for the radial diagram and splitting displacement $\bar{\mathbf{u}}_2$. The normalised objective function reported is $\tilde{W}_c/W = 11.3\%$. The settlement induces the two halves of the dome to tilt inwards, increasing the pressure onto the central strip of the dome orthogonal to the settlements, which assumes a maximum thrust state. The increased force is evident by the increased length of the corresponding edges in Γ^* (see T_i). For the split displacement $\bar{\mathbf{u}}_2$, $\tilde{W}_c$ corresponds to the sum of the $x-$components of the reaction forces, which is represented by the height of Γ^*, as noted in Fig. 3b. This height is decreased due to the new internal force distribution.

The same displacement field $\bar{\mathbf{u}}_2$ is imposed onto the modified diagram and the results are depicted in Fig. 3c. The normalised objective function reported is $\tilde{W}_c/W = 8.5\%$, which is 25% less than the results obtained with the radial diagram. For this solution, the inclined meridians get activated (e.g., T_i), enabling an alternative force flow oblique to the applied settlement. This new force flow elongates Γ^* and reduces its height, and hence $\tilde{W}_c$. Regarding the internal force distribution, hoop forces also vanish toward the supports, suggesting possible inclined meridian cracks. Moreover, near the central strip, the network touches the extrados into two crack lines suggesting cracks in the intrados due to the two halves leaning inwards. Given the reduction of $\tilde{W}_c$, this internal stress state is a better fit for the imposed spitting displacement. It is a valid solution from a lower-bound limit analysis standpoint which has been achieved by analysing the problem with a different form diagram.

4.3. Cross and pavillion vaults

In this section, a cross and a pavillion vault are considered. The parameters defining the cross-sectional geometry of these structures are presented in Fig. 4a, after [26]. The vaults are generated through the intersection of two barrel vaults with the same semicircular profile ($r/l_0 = 0.5$), with a springing angle $\beta = 30°$ and a thickness over span $t/s = 0.05$.

The cross vault is subjected to a corner horizontal outward displacement $\bar{\mathbf{u}}_1$ (Fig. 4b). The diagram used to describe the internal force flow is an orthogonal grid with main diagonals following the vault's creases. Supports are assigned only at the corners of the vault, and the set of independent edges used in the problem is highlighted in blue at Fig. 4b.

The pavillion vault is subjected to a unitary outward sliding of one of its line supports $\bar{\mathbf{u}}_2$ (Fig. 4c). The form diagram used is a similar orthogonal diagram in which 56 supports are considered along the boundaries. The set of independent edges used in the analysis is highlighted in Fig. 4c.

The minimum complementary energy for the cross vault problem is depicted in Fig. 5a. The value of the normalised objective function is $\tilde{W}_c/W = 20.4\%$. The outward diagonal displacement reflects a spreading of the webs crossing the pulled diagonal. This spreading results in two crack lines crossing that diagonal, obtained by connecting adjacent vertices touching the extrados (green). Uneven horizontal thrusts are observed, decreasing the horizontal thrust in the displaced corner (T_i) and increasing the pressure applied to the opposite diagonal (T_j). This uneven horizontal reaction is reflected in the elongated shape of Γ^*. Graphically, the value of $\tilde{W}_c$ corresponds to the length of T_i as the horizontal component of that reaction is parallel to the foundation

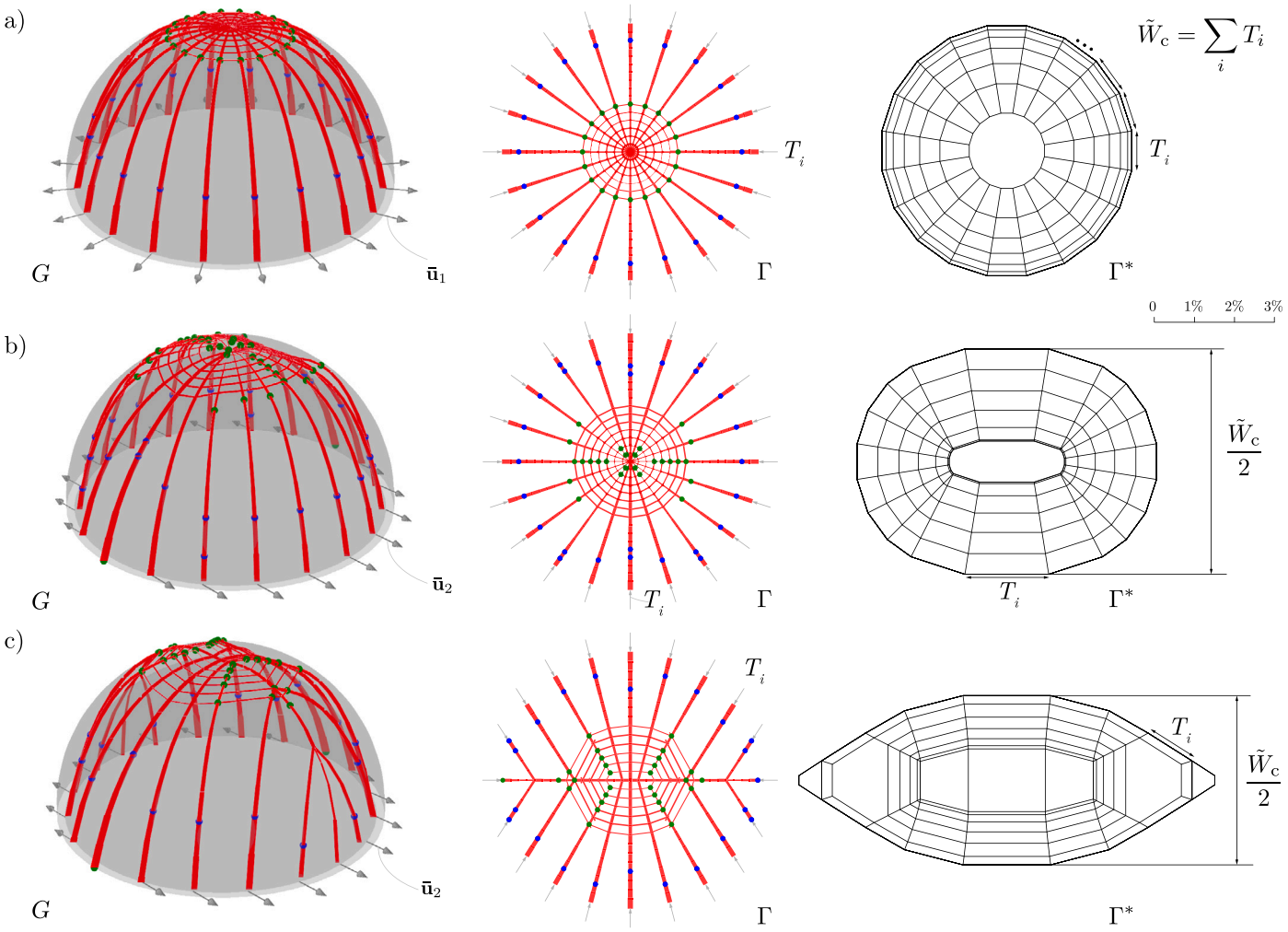

Fig. 3. Thrust network (G), form (Γ) and force (Γ^*) diagrams for the minimum complementary energy in the dome assuming (a) outward displacement $\bar{\mathbf{u}}_1$ and radial diagram, (b) splitting displacement $\bar{\mathbf{u}}_2$ and radial diagram and (c) displacement $\bar{\mathbf{u}}_2$ and the modified diagram. (For interpretation of the references to colour in this figure legend, the reader is referred to the web version of this article.)

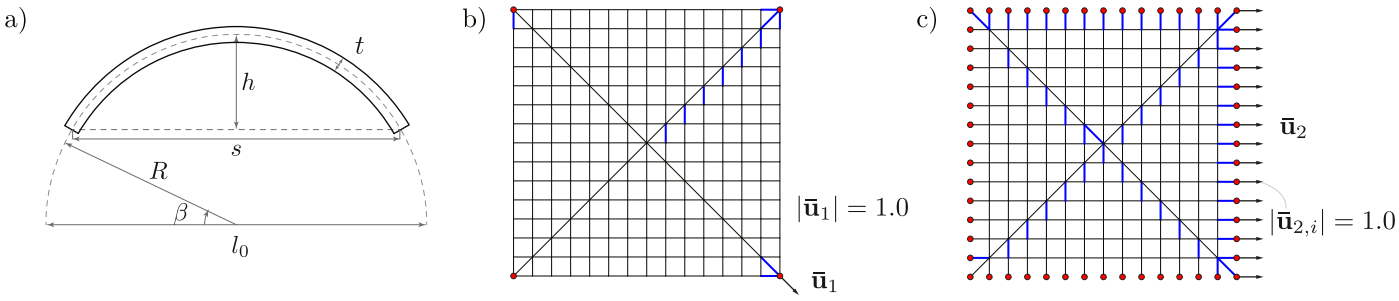

Fig. 4. (a) Cross-section and parameters to construct the cross and pavillion vaults. (b) Orthogonal form diagram and corner displacement $\bar{\mathbf{u}}_1$. (c) Orthogonal form diagram with continuous supports and displacement $\bar{\mathbf{u}}_2$. Independent edges are shown in blue and supports in red. (For interpretation of the references to colour in this figure legend, the reader is referred to the web version of this article.)

displacement. Qualitatively, the crack lines in the webs described here follow the crack pattern obtained in cross vaults with Discrete Element Modelling (DEM) in [50].

The minimum complementary energy for the pavillion vault problem is depicted in Fig. 5b. The value of the normalised objective function is $\tilde{W}_c/W = 2.6\%$. The support movement suggests crack lines in the intrados on the web adjacent to the settlement. The force paths parallel to the settlement assume a minimum thrust behaviour (e.g., T_i) or vanish. Consequently, the loads flow in the perpendicular direction in which the force paths assume a maximum thrust configuration (e.g., T_j). This is evident in Γ^*, where the magnitudes of T_i and T_j are highlighted, and the diagram assumes an elongated shape having a low height and hence low $\tilde{W}_c$. A similar geometry has been analysed in [51] considering a DEM approach in which the web cracks suggested by the present model have been also obtained. However, in [51], only the portion near the support is observed to crack since, due to the friction among the elements, the opposite web is not affected.

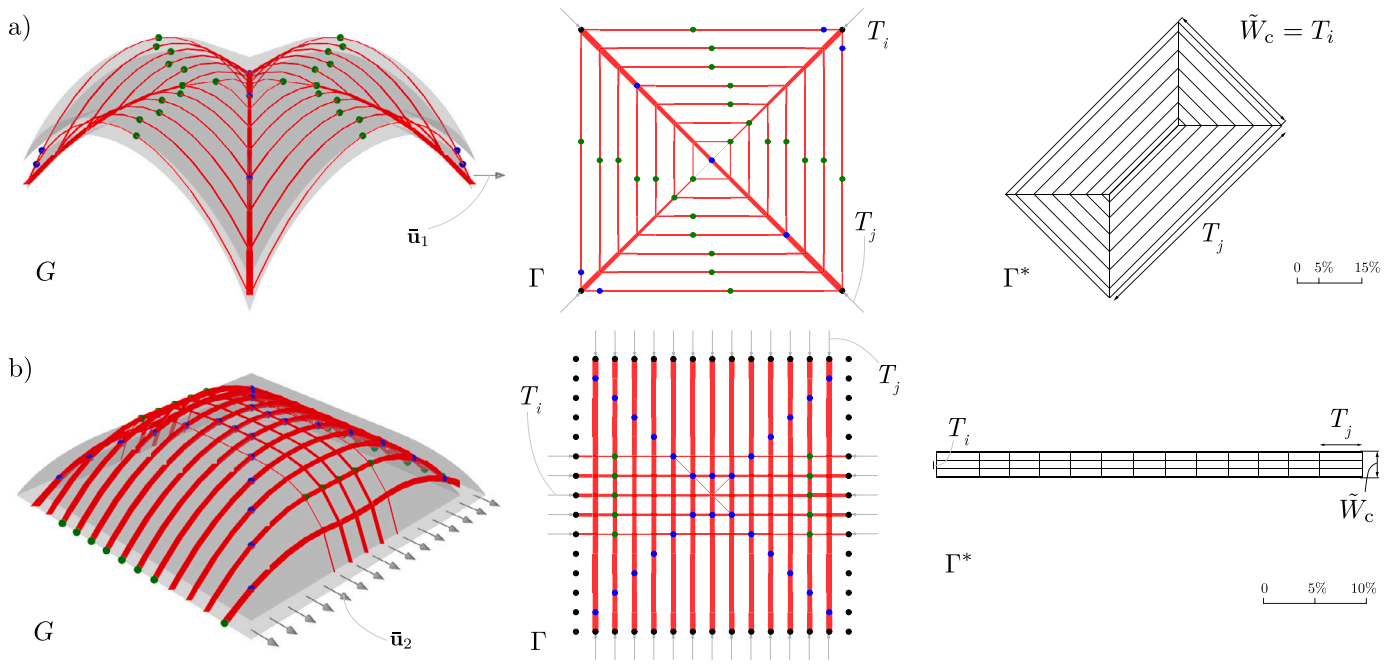

Fig. 5. Thrust network (G), form (Γ) and force (Γ^*) diagrams for the minimum complementary energy in (a) the cross vault subjected to corner displacement $\bar{\mathbf{u}}_1$, and (b) pavillion vault subjected to outward displacement $\bar{\mathbf{u}}_2$. (For interpretation of the references to colour in this figure legend, the reader is referred to the web version of this article.)

4.4. Combined effects of settlements and horizontal loads

This section revisits the pavillion vault from Section 4.3 to show the coupled effects of horizontal loads and foundation settlements. The horizontal load is applied to the vertices of the network in the $x-$direction. A horizontal load multiplier $\lambda_h = 0.30$ is considered, which means that the horizontal force component at each vertex has a magnitude equal to 30% of its the lumped self-weight. Horizontal load multipliers are often used to approximate the effect of earthquakes in masonry vaults [52]. By combining settlements and horizontal loads, e.g., the leaning of supporting walls during an earthquake can be modelled.

The minimum complementary energy solution for the pavillion vault problem with $\lambda_h = 0.30$ is depicted in Fig. 6. The objective function value is $\tilde{W}_c/W = 28.9\%$. The thrust network obtained is tilted against the horizontal loads, as shown in the main section (Fig. 6b). Furthermore, the loads flow orthogonally to $\bar{\mathbf{u}}_2$ and to the corners, alleviating the thrust acting on the displacing line support. This solution not only shows that the pavillion vault studied can support the horizontal loading applied, as a consequence of the Limit Analysis' Safe Theorem, but it also enables an exploration of the domain of admissible solutions for particular movements of the supports. Further optimisation and variation of the form diagram topology could be envisaged to model the reduction of the thrust over the settled supports.

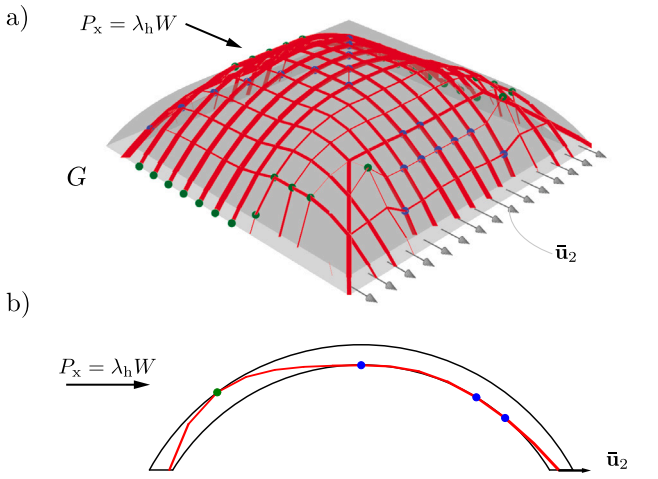

Fig. 6. Results obtained for the pavillion vault subjected to boundary outward displacement and horizontal load with a multiplier $\lambda_h = 0.30$. (a) Perspective and (b) main sectional view.

5. Discussion

The results presented allow an investigation of internal stress states following small foundation displacements in no-tensile rigid materials, such as masonry structures. The results suggest potential crack regions arising at the onset of the motion activated by the settlements. Cracks are indicated in the points where the network touches the boundary, opposite to the intra- or extrados, as in the arch (Fig. 1), and by portions in which the compressive forces in the network vanish, indicating possible "wrinkle" fractures, or smeared cracks [13,53,54], as in the dome (Fig. 3). For 3D problems, an indication of crack lines is provided by connecting neighbouring vertices touching sectional limits.

The method, however, is limited to suggesting where cracks will form, as the appearance of fractures also relates to the stereotomy of the blocks, and other mechanical properties (e.g., friction), which are not considered by the present methodology. The method also does not account for the nonlinear effects due to large deformations (e.g., see [29,51]) and is dependent on the geometry of the form diagram. The form diagram selection should follow the structures' geometric features, prescribed displacement and loading conditions. Strategies to improve the selection of appropriate form diagrams include analysing initial stress states with the help of force diagrams (Fig. 3) and providing additional force paths to the supports, e.g., by adding diagonals to the form diagram as in [26]. Moreover, the combination with feature-based topology generative methods, as in [55] could enlarge the space of suitable form diagrams. From the nonlinear nature of the problem, the optimisation is also prone to local minima, which can be reduced by combining it with evolutionary methods, as in [42].

6. Conclusions

In this paper, the search for admissible stress states in masonry structures compatible with foundation settlements in equilibrium with general loading conditions is performed by coupling Thrust Network Analysis (TNA) with an energy-based criterion. This search is executed through a constrained nonlinear optimisation problem in which the objective function minimises the complementary energy. This paper derives the complementary energy expression for a general network in terms of force densities and support elevations. The expression is then specialised in the case of the normal, rigid, no-tension material (NRNT), where it is reduced to the minimisation of the opposite work of the reaction forces. The problem is formulated and solved with interior point methods whose gradient analytical expressions are also derived. A novel python package named *compas_tno* has been developed to perform the analysis enabling the assessment of vaulted masonry structures with TNA.

The proposed methodology allows for searching among the infinite admissible stress states, the ones compatible with the imposed displacements. It applies to three-dimensional structures subjected to vertical and horizontal loads. By finding such compatible stress states, potential crack regions arising at the onset of the motion can be identified. Understanding the effects of foundation displacements in masonry is important as it constitutes one of the primary reasons for damages and collapse in such structures.

The merit of the present formulation is that the input required is simple, and it provides a practical outcome to evaluate the mechanics of three-dimensional vaulted systems even when non-detailed information is available because of constraints on time and budget. Applications include investigating crack patterns for plausible foundation displacements or even the inverse analysis by searching among different support displacements that best match the observed cracks and distortions in the masonry. Further will focus on investigating different form diagram topologies, especially those following existing crack lines observed in damaged structures.

Funding

This work was supported by the SNSF — Swiss National Science Foundation. Project grant #178953: “Practical Stability Assessment Strategies for Vaulted Unreinforced Masonry Structures”.

Declaration of competing interest

The authors declare that they have no known competing financial interests or personal relationships that could have appeared to influence the work reported in this paper.

Data availability

Data will be made available on request.

References

[1] S. Huerta, The analysis of masonry architecture: A historical approach, Archit. Sci. Rev. 51 (4) (2008) 297–328.
[2] S. Huerta, Mechanics of masonry vaults: the equilibrium approach, in: P. Lourenço, P. Roca (Eds.), Historical Constructions. Possibilities of Numerical and Experimental Techniques, Universidade do Minho, Guimarães, 2001, pp. 47–70.
[3] J. Ochsendorf, Collapse of masonry structures (Ph.D. thesis), University of Cambridge, Cambridge, 2002.
[4] H.V. Shin, C.F. Porst, E. Vouga, J. Ochsendorf, F. Durand, Reconciling elastic and equilibrium methods for static analysis, ACM Trans. Graph. 35 (2) (2016) 1–16, http://dx.doi.org/10.1145/2835173, URL https://dl.acm.org/doi/10.1145/2835173.
[5] A. Tralli, C. Alessandri, G. Milani, Computational methods for masonry vaults: A review of recent results, The Open Civ. Eng. J. 8 (1) (2014) 272–287, http://dx.doi.org/10.2174/1874149501408010272.
[6] J. Heyman, The stone skeleton, Int. J. Solids Struct. 2 (2) (1966) 249–279, http://dx.doi.org/10.1016/0020-7683(66)90018-7.
[7] F. Fraternali, M. Angelillo, A. Fortunato, A lumped stress method for plane elastic problems and the discrete-continuum approximation, Int. J. Solids Struct. 39 (25) (2002) 6211–6240, http://dx.doi.org/10.1016/S0020-7683(02)00472-9.
[8] F. Fraternali, A thrust network approach to the equilibrium problem of unreinforced masonry vaults via polyhedral stress functions, Mech. Res. Commun. 37 (2) (2010) 198–204, http://dx.doi.org/10.1016/j.mechrescom.2009.12.010.
[9] A. Montanino, C. Olivieri, G. Zuccaro, M. Angelillo, From stress to shape: Equilibrium of cloister and cross vaults, Appl. Sci. 11 (9) (2021) 3846, http://dx.doi.org/10.3390/app11093846.
[10] N.A. Nodargi, P. Bisegna, Collapse capacity of masonry domes under horizontal loads: A static limit analysis approach, Int. J. Mech. Sci. 212 (2021) 106827, http://dx.doi.org/10.1016/j.ijmecsci.2021.106827.
[11] N.A. Nodargi, P. Bisegna, A finite difference method for the static limit analysis of masonry domes under seismic loads, Meccanica 57 (1) (2022) 121–141, http://dx.doi.org/10.1007/s11012-021-01414-3.
[12] G. Del Piero, Limit analysis and no-tension materials, Int. J. Plast. 14 (1) (1998) 259–271, http://dx.doi.org/10.1016/S0749-6419(97)00055-7.
[13] M. Angelillo, Practical applications of unilateral models to masonry equilibrium, in: M. Angelillo (Ed.), Mechanics of Masonry Structures, vol. 551, 10.1007/978-3-7091-1774-3_4, Springer Vienna, 2014, pp. 109–210, http://dx.doi.org/10.1007/978-3-7091-1774-3_4.
[14] G. Poleni, Memorie Istoriche Della Gran Cupola Del Tempio Vaticano, E de’Danni Di Essa, E de’Ristoramenti Loro, Divise in Libri Cinque ..., Stamperia del Seminario, Padova, 1748, http://dx.doi.org/10.3931/e-rara-13403.
[15] H. Moseley, On the theory of the arch, in: J. Weale (Ed.), Theory, Practice and Architecture of Bridges, vol. I, Architectural Library, London, 1843, pp. 1–72.
[16] G. Ungewitter, Lehrbuch Der Gotischen Konstruktionen, T.O. Weigel Nachfolger, Leipzig, 1890.
[17] W.S. Wolfe, Graphical Analysis: A Text Book in Graphic Statics, McGraw-Hill Book Company, New York, 1921.
[18] D. Aita, R. Barsotti, S. Bennati, A parametric study of masonry domes equilibrium via a revisitation of the durand-claye method, in: Proceedings of the 7th International Conference on Computational Methods in Structural Dynamics and Earthquake Engineering (COMPDYN 2015), Institute of Structural Analysis and Antiseismic Research School of Civil Engineering National Technical University of Athens (NTUA) Greece, 2019, pp. 663–672, http://dx.doi.org/10.7712/120119.6947.19313.
[19] J. Zessin, W. Lau, J. Ochsendorf, Equilibrium of cracked masonry domes, Proc. Inst. Civ. Eng. Eng. Comput. Mech. 163 (3) (2010) 135–145, http://dx.doi.org/10.1680/eacm.2010.163.3.135.
[20] M. Angelillo, C. Olivieri, M.J. DeJong, A new equilibrium solution for masonry spiral stairs, Eng. Struct. 238 (2021) 112176, http://dx.doi.org/10.1016/j.engstruct.2021.112176.
[21] D. O’Dwyer, Funicular analysis of masonry vaults, Comput. Struct. 73 (1) (1999) 187–197, http://dx.doi.org/10.1016/S0045-7949(98)00279-X.
[22] P. Block, J. Ochsendorf, Thrust network analysis: A new methodology for three-dimensional equilibrium, J. Int. Assoc. Shell Spatial Struct. 48 (3) (2007) 167–173, URL https://www.ingentaconnect.com/content/iass/jiass/2007/00000048/00000003/art00011.
[23] F. Marmo, L. Rosati, Reformulation and extension of the thrust network analysis, Comput. Struct. 182 (2017) 104–118.
[24] P. Block, L. Lachauer, Three-dimensional funicular analysis of masonry vaults, Mech. Res. Commun. 56 (2014) 53–60, http://dx.doi.org/10.1016/j.mechrescom.2013.11.010.
[25] R. Maia Avelino, A. Iannuzzo, T. Van Mele, P. Block, Assessing the safety of vaulted masonry structures using thrust network analysis, Comput. Struct. 257 (2021) 106647, http://dx.doi.org/10.1016/j.compstruc.2021.106647.
[26] R. Maia Avelino, A. Iannuzzo, T. Van Mele, P. Block, Parametric stability analysis of groin vaults, Appl. Sci. 11 (8) (2021) 3560, http://dx.doi.org/10.3390/app11083560.
[27] M. Bruggi, A constrained force density method for the funicular analysis and design of arches, domes and vaults, Int. J. Solids Struct. 193–194 (2020) 251–269, http://dx.doi.org/10.1016/j.ijsolstr.2020.02.030.
[28] M. Bruggi, B.A. Lógó, Z. Deák, Funicular analysis of ribbed masonry vaults: A case study, Int. J. Archit. Heritage (2021) 1–15, http://dx.doi.org/10.1080/15583058.2021.1910879.
[29] J. Ochsendorf, The masonry arch on spreading supports, Struct. Eng. 84 (2006) 29–35, URL https://www.istructe.org/journal/volumes/volume-84-(published-in-2006)/issue-2/the-masonry-arch-on-spreading-supports/.
[30] M. Como, Statics of Historic Masonry Constructions, in: Springer Series in Solid and Structural Mechanics, vol. 1, Springer Berlin Heidelberg, Berlin, Heidelberg, 2013.
[31] M. Angelillo, A. Fortunato, A. Gesualdo, A. Iannuzzo, G. Zuccaro, Rigid block models for masonry structures, Int. J. Masonry Res. Innov. 3 (4) (2018) 349–368, http://dx.doi.org/10.1504/IJMRI.2018.095701.
[32] A. Iannuzzo, A. Dell’Endice, T. Van Mele, P. Block, Numerical limit analysis-based modelling of masonry structures subjected to large displacements, Comput. Struct. 242 (2021) 106372, http://dx.doi.org/10.1016/j.compstruc.2020.106372.

[33] A. Iannuzzo, T. Van Mele, P. Block, Piecewise rigid displacement (PRD) method: a limit analysis-based approach to detect mechanisms and internal forces through two dual energy criteria, Mech. Res. Commun. 107 (2020) 103557, http://dx.doi.org/10.1016/j.mechrescom.2020.103557.

[34] A. Gesualdo, B. Calderoni, A. Iannuzzo, A. Fortunato, M. Monaco, Minimum energy strategies for the in-plane behaviour of masonry, Frattura Integr. Strut. 14 (51) (2019) 376–385, http://dx.doi.org/10.3221/IGF-ESIS.51.27.

[35] A. Fortunato, A. Gesualdo, I. Mascolo, M. Monaco, P-bézier energy optimisation for elastic solutions of masonry-like panels, Int. J. Masonry Res. Innov. 7 (1) (2022) 113, http://dx.doi.org/10.1504/IJMRI.2022.119857.

[36] H.J. Schek, The force density method for form finding and computation of general networks, Comput. Methods Appl. Mech. Engrg. 3 (1) (1974) 115–134, http://dx.doi.org/10.1016/0045-7825(74)90045-0.

[37] T. Van Mele, P. Block, Algebraic graph statics, CAD Comput. Aided Des. 53 (2014) 104–116, http://dx.doi.org/10.1016/j.cad.2014.04.004.

[38] S. Pellegrino, Structural computations with the singular value decomposition of the equilibrium matrix, Int. J. Solids Struct. 30 (21) (1993) 3025–3035, http://dx.doi.org/10.1016/0020-7683(93)90210-X.

[39] M. Fantin, T. Ciblac, Extension of thrust network analysis with joints consideration and new equilibrium states, Int. J. Space Struct. 31 (2) (2016) 190–202, http://dx.doi.org/10.1177/0266351116661814.

[40] N. Nodargi, P. Bisegna, A new computational framework for the minimum thrust analysis of axisymmetric masonry domes, Eng. Struct. 234 (2021) 111962, http://dx.doi.org/10.1016/j.engstruct.2021.111962.

[41] J. Heyman, The Stone Skeleton: Structural Engineering of Masonry Architecture, Cambridge University Press, Cambridge, 1995, http://dx.doi.org/10.1017/CBO9781107050310, URL 10.1017/CBO9781107050310.

[42] A. Liew, D. Pagonakis, T. Van Mele, P. Block, Load-path optimisation of funicular networks, Meccanica 53 (1) (2018) 279–294, http://dx.doi.org/10.1007/s11012-017-0714-1.

[43] A. Liew, R. Avelino, V. Moosavi, T. Van Mele, P. Block, Optimising the load path of compression-only thrust networks through independent sets, Struct. Multidiscip. Optim. 60 (1) (2019) 231–244, http://dx.doi.org/10.1007/s00158-019-02214-w.

[44] W.F. Baker, L.L. Beghini, A. Mazurek, J. Carrion, A. Beghini, Maxwell's reciprocal diagrams and discrete Michell frames, Struct. Multidiscip. Optim. 48 (2) (2013) 267–277, http://dx.doi.org/10.1007/s00158-013-0910-0.

[45] A. Wächter, L.T. Biegler, On the implementation of an interior-point filter line-search algorithm for large-scale nonlinear programming, Math. Program. 106 (1) (2006) 25–57, http://dx.doi.org/10.1007/s10107-004-0559-y.

[46] R. Maia Avelino, COMPAS TNO: An implementation of constrained optimisation to thrust networks for the assessment of masonry structure, 2022, URL https://blockresearchgroup.github.io/compas_tno.

[47] S. Huerta, Galileo was wrong: The geometrical design of masonry arches, Nexus Netw. J. 8 (2) (2006) 25–52, http://dx.doi.org/10.1007/s00004-006-0016-8.

[48] A. Iannuzzo, A new rigid block model for masonry structures (Ph.D. thesis), Universitá degli Studi di Napoli Federico II, Napoli, 2018, URL http://www.fedoa.unina.it/11732/.

[49] P. Zampieri, F. Faleschini, M.A. Zanini, N. Simoncello, Collapse mechanisms of masonry arches with settled springing, Eng. Struct. 156 (2018) 363–374, http://dx.doi.org/10.1016/j.engstruct.2017.11.048.

[50] J. McInerney, M.J. DeJong, Discrete element modeling of groin vault displacement capacity, Int. J. Archit. Heritage 9 (8) (2015) 1037–1049, http://dx.doi.org/10.1080/15583058.2014.923953.

[51] A. Dell'Endice, A. Iannuzzo, M.J. DeJong, T. Van Mele, P. Block, Modelling imperfections in unreinforced masonry structures: Discrete element simulations and scale model experiments of a pavilion vault, Eng. Struct. 228 (2021) 111499, http://dx.doi.org/10.1016/j.engstruct.2020.111499.

[52] M.J. DeJong, Seismic Assessment Strategies for Masonry Structures (Ph.D. thesis), MIT, Cambridge, 2009, URL http://hdl.handle.net/1721.1/49538.

[53] H.R. Lotfi, P.B. Shing, An appraisal of smeared crack models for masonry shear wall analysis, Comput. Struct. 41 (3) (1991) 413–425, http://dx.doi.org/10.1016/0045-7949(91)90134-8.

[54] W. Wong, S. Pellegrino, Wrinkled membranes, Part II: Analytical models, J. Mech. Mater. Struct. 1 (1) (2006) 27–61, http://dx.doi.org/10.2140/jomms.2006.1.27.

[55] R. Oval, M. Rippmann, R. Mesnil, T. Van Mele, O. Baverel, P. Block, Feature-based topology finding of patterns for shell structures, Autom. Constr. 103 (May 2018) (2019) 185–201, http://dx.doi.org/10.1016/j.autcon.2019.02.008.